

Dynamical phases in a one-dimensional chain of heterospecies Rydberg atoms with next-nearest-neighbor interactions

Jing Qian,^{1,2,*} Lu Zhang,¹ Jingjing Zhai,¹ and Weiping Zhang^{1,2}

¹*Quantum Institute for Light and Atoms, Department of Physics, East China Normal University, Shanghai 200062, People's Republic of China*

²*Collaborative Innovation Center of Extreme Optics, Shanxi University, Taiyuan, Shanxi 030006, People's Republic of China*

(Received 24 June 2015; published 8 December 2015)

We theoretically investigate the dynamical phase diagram of a one-dimensional chain of laser-excited two-species Rydberg atoms. The existence of a variety of unique dynamical phases in the experimentally achievable parameter region is predicted under the mean-field approximation, and the change in those phases when the effect of the next-nearest-neighbor interaction is included is further discussed. In particular, we find that the competition of the strong Rydberg-Rydberg interactions and the optical excitation imbalance can lead to the presence of complex multiple chaotic phases, which are highly sensitive to the initial Rydberg-state population and the strength of the next-nearest-neighbor interactions.

DOI: [10.1103/PhysRevA.92.063407](https://doi.org/10.1103/PhysRevA.92.063407)

PACS number(s): 32.80.Ee, 32.80.Rm, 32.80.Qk, 34.20.Cf

I. INTRODUCTION

Ultracold atoms combined with optical lattices [1–5] can give rise to a clean and controllable platform for simulating and studying quantum many-body physics [6], capably demonstrating various quantum phases and even the dynamics of phase transitions. Recently, an efficient optical-lattice trap for Rydberg atoms was realized in experiments [7], extending quantum simulation research to the realm of Rydberg atom physics. Differently from the commonly used ground-state atoms, the giant dipole moment induced by highly excited atomic states results in an interaction of unprecedented magnitude and range between two Rydberg atoms, that is, the Rydberg-Rydberg interaction (RRI) [8], which could further lead to the Rydberg blockade effect [9]. This characteristic of Rydberg atoms is conducive to simulation of strongly correlated quantum many-body systems [10–13] and to realization of nonequilibrium quantum phase transitions [14].

So far, little attention has been paid to the heterospecies Rydberg lattice gas, most research has focused on the dynamical phases of single-species Rydberg lattice gases when both strong RRIs and spontaneous emission effects are present [15–20]. For a single-species Rydberg lattice gas, intrinsically, only the strong RRIs in the nearest-neighbor (NN) sites should be considered [12], since the long-range RRIs due to next-nearest-neighbor (NNN) interactions are already orders of magnitude smaller [21]. However, things will be quite different for the heterospecies case. Here the heterospecies case can be two Rydberg atoms of different atomic species [22] or two same-species atoms occupied in different Rydberg hyperfine states [23]. The different excitation frequencies would disrupt the Rydberg blockade mechanism as well as those phases existing in the single-species case. Moreover, the RRIs between heterospecies Rydberg atoms can vary by orders of magnitude [22,24], which means the NNN interaction between two Rydberg atoms of the same species could be comparable to the NN interaction between heterospecies atoms, and vice versa. So the effect of NNN interaction deserves to be discussed in the lattice model of heterospecies Rydberg

atoms. Especially, the importance of NNN interactions has been demonstrated in a recent experiment showing that the excitation dynamics could be significantly different from the common cases [25].

In the present work we explore the dynamical phase diagram of a one-dimensional (1D) chain of heterospecies Rydberg atoms in an open environment. The Rydberg atoms of two species are alternatively arranged in the 1D optical lattice, with internal states being subjected to laser pumping and spontaneous decay. By the mean-field approximation (MFA), we predict the presence of a rich variety of dynamical phases, involving three stable phases—the antiferromagnetic phase, the bistable antiferromagnetic phase, and the tristable antiferromagnetic phase—and unstable phases whose dynamics can change from ordinary oscillation to chaos in the strong-RRI case. No uniform phase that presents in the single-species case is found due to the heterospecies atomic excitations. We investigate the impacts of repulsive and attractive NNN interactions on these phases and find that stable phases prefer repulsive ones. Especially, the chaotic phase has been shown to have a high sensitivity to NNN interactions, which verifies the necessity of including them in our model of a heterospecies Rydberg atom chain.

The paper is organized as follows: In Sec. II we report a scheme for presenting the exciting dynamics of a heterospecies Rydberg atom chain and derive basic master equations, from which the stationary-state solutions can be solved. In Secs. III and IV, we investigate the change in phase diagrams without and with the effect of NNN RRIs, respectively. In Sec. V, we compare the different influences of repulsive and attractive NNN RRIs on the chaotic phase. Finally, a brief conclusion is given in Sec. VI.

II. SCHEME AND MASTER EQUATION

As shown in Fig. 1, the system we propose consists of a chain formed by two-species Rydberg atoms, trapped in a regular 1D lattice. Efficient trapping of single rubidium atoms in a 1D optical lattice was initially realized in Ref. [7], and the loading of different atoms can use a species-selective optical lattice [26,27]. Here we assume that the atoms of species *A* and *B* are alternatively arranged at the lattice sites with a filling

*jqian1982@gmail.com

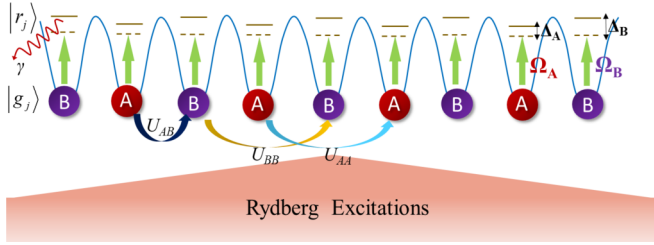


FIG. 1. (Color online) Schematic of two-species atoms (A and B) trapped in a 1D optical lattice. Atoms are excited from the ground state $|g_j\rangle$ to the Rydberg state $|r_j\rangle$ by different laser Rabi frequencies Ω_A and Ω_B . Simultaneously, they are suffering from nonignorable spontaneous decay γ . The NN and NNN RRI strengths are, respectively, labeled U_{AB} and $U_{AA(BB)}$, representing the interspecies short-distance and intraspecies long-distance interactions. The one-photon detunings between the laser frequency and the atomic transition frequency are denoted Δ_A and Δ_B , differently.

factor of one atom per site and the hopping of an atom into an adjacent filled site is forbidden by the large depth of the lattice. Each atom j is modeled as a two-level configuration, composed of a ground state $|g_j\rangle$ and a Rydberg state $|r_j\rangle$, whose transition is performed by an off-resonant laser beam with Rabi frequency Ω_j and one-photon detuning Δ_j . For the lattice structure here, if we replace the site index with the atom species inside, i.e., $j = A$, we have $j \pm 1 = B$ and $j \pm 2 = A$. It is also noteworthy that the assumption of two-species atoms can be equivalent to a scheme of same-ground-state atoms excited to two different Rydberg hyperfine states [23].

In the absence of external fields, two atoms prepared in the nS -Rydberg states generally interact via a nonresonant van der Waals (vdW) RRI, described by $U_{ij} = C_6^{(ij)}/|x_i - x_j|^6$, where $x_{i(j)}$ represents the position of atom $i(j)$ in the lattice and $C_6^{(ij)}$ the coefficient for dispersion. To our knowledge, $C_6^{(ij)}$ is well defined [28] and measured [29] in the case of same species of atoms, such as Rb-Rb, Na-Na, K-K, Li-Li, and Cs-Cs. However, as for different atomic species or different hyperfine states, $C_6^{(ij)}$ changes significantly [22,30,31]. In this paper, we focus on two vdW-type interactions: (i) the interspecies interaction between NN sites of different atomic species, denoted $U_{j,j\pm 1} = U_{AB}$; and (ii) the intraspecies interaction between NNN sites of the same atomic species, denoted $U_{j,j\pm 2} = U_{AA}$ or U_{BB} .

Here we consider both NN and NNN interactions, since the long-range NNN RRIs between same-species atoms are no longer negligible once the intraspecies interactions are much stronger than the interspecies ones. Other longer-range interactions, such as the next-next-nearest-neighbor interaction, are smaller than the NNN interactions by at least a factor of $(C_6^{(AB)}/C_6^{(AA(BB))})(2/3)^6$ and, therefore, are negligible here. Then in a frame rotating at the laser frequency, the Hamiltonian of the system reads

$$\mathcal{H} = \sum_j \left(\mathcal{H}_j + \sum_{k=j\pm 1, j\pm 2} U_{jk} |r_j\rangle \langle r_j| \otimes |r_k\rangle \langle r_k| \right), \quad (1)$$

where $\mathcal{H}_j = -\Delta_j |r_j\rangle \langle r_j| + \Omega_j (|g_j\rangle \langle r_j| + |r_j\rangle \langle g_j|)$, accounting for the single atom-laser coupling; $U_{jk} = U_{AB}$ for NN

RRIs with $k = j \pm 1$; and $U_{jk} = U_{AA}$ or U_{BB} for NNN RRIs with $k = j \pm 2$. The system dynamics is described by the master equation of the density matrix operator ρ [32],

$$\partial_t \rho = -i[\mathcal{H}, \rho] + \mathcal{L}[\rho], \quad (2)$$

where the effect of the spontaneous decay from the unstable state $|r_j\rangle$ at the rate γ is included by the Lindblad operator,

$$\mathcal{L}[\rho] = \gamma \sum_j \left(-\frac{1}{2} \{ |r_j\rangle \langle r_j|, \rho \} + |g_j\rangle \langle r_j| \rho |r_j\rangle \langle g_j| \right). \quad (3)$$

Due to the enormous Hilbert space, it is hard to perform an exact numerical simulation of the above chain model with a large atom number, so we apply the MFA here. Compared with the method of Monte Carlo simulations [18], as the interatomic quantum correlation and its fluctuations are ignored, the MFA may fail to predict the phase transition under the same system parameters or to obtain the exact boundary in the phase diagram. However, the MFA is still regarded as a reliable and adequate tool to qualitatively describe the phase diagram and, at least, to predict the existence of different kinds of steady-state phases [15–17]. Under the MFA we can neglect the intersite quantum correlation and factorize the density matrix at each site, $\rho = \otimes_j \rho_j$ [33,34]. For atom j , the second term in Eq. (1) should be replaced with $|r_j\rangle \langle r_j| \sum_{k=j\pm 1, j\pm 2} \rho_{k,rr}$, where $\rho_{k,ab=gg,gr,rg,rr}$ represents the density matrix elements for a two-level atom at site k . Furthermore, we consider two sublattices filled with atoms A and B, respectively, as shown in Fig. 1. The excitation probabilities of their Rydberg states are different. This is why the uniform phase cannot be found here. We assume that the NNN interactions between same-species atoms are also relatively weak so the induced blockade effect is ignored.

With all the approximations and assumptions above, the motional equations of the density matrix can be derived as

$$\dot{\rho}_{A,rr} = 2\Omega_A \rho_{A,gr}^I - \rho_{A,rr}, \quad (4)$$

$$\dot{\rho}_{A,gr} = i\Delta_{A,\text{eff}} \rho_{A,gr} + i\Omega_A (1 - 2\rho_{A,rr}) - \frac{1}{2} \rho_{A,gr}, \quad (5)$$

$$\dot{\rho}_{B,rr} = 2\Omega_B \rho_{B,gr}^I - \rho_{B,rr}, \quad (6)$$

$$\dot{\rho}_{B,gr} = i\Delta_{B,\text{eff}} \rho_{B,gr} + i\Omega_B (1 - 2\rho_{B,rr}) - \frac{1}{2} \rho_{B,gr}, \quad (7)$$

where all the frequencies are scaled by the decay rate γ and the effective detunings are defined as

$$\Delta_{A,\text{eff}} = \Delta_A - U_{AA} \rho_{A,rr} - U_{AB} \rho_{B,rr}, \quad (8)$$

$$\Delta_{B,\text{eff}} = \Delta_B - U_{BB} \rho_{B,rr} - U_{AB} \rho_{A,rr}, \quad (9)$$

from which we find that the bare detunings are shifted by two nonlinear terms that are proportional to the NN and NNN interactions, respectively.

In principle, via an adjustment of bare detunings Δ_A and Δ_B , one can compensate for the density-dependent frequency shifts caused by RRIs so that the effective detunings may vanish. This is the internal working of the antiblockade effect in a Rydberg chain of single-species atoms [35,36]. However, both intraspecies and interspecies RRIs work here,

TABLE I. Eight types of possible dynamical phases obtained in a chain of heterospecies Rydberg atoms with the impact of NN and NNN RRIs. PRN represents the total number of physical roots of Eqs. (10) and (11) (see text), and SRN and USRN stand for the number of stable and unstable roots, respectively. The phases are stable if SRN is larger than USRN. The three stable phases are labeled nAF ; the five unstable phases, CHn .

	Phase									
	Stable			Unstable						
PRN	1	3	5	1	3	3	5	5		
SRN	1	2	3	0	0	1	1	2		
USRN	0	1	2	1	3	2	4	3		
Label	1AF	2AF	3AF	CH1	CH2	CH3	CH4	CH5		

which induces a complicated nonlinear coupling, making the compensation effect elusive.

We begin our discussion of the dynamical phase diagram of such an open system by studying the features of the steady-state solutions of Eqs. (4)–(7). When we set $\dot{\rho}_{k,r(g)r} = 0$, these equations can be simplified to a pair of coupled stationary equations,

$$(\Delta_{A,\text{eff}}^s)^2 = \frac{4\Omega_A^2(1 - 2\rho_{A,rr}^s) - \rho_{A,rr}^s}{4\rho_{A,rr}^s}, \quad (10)$$

$$(\Delta_{B,\text{eff}}^s)^2 = \frac{4\Omega_B^2(1 - 2\rho_{B,rr}^s) - \rho_{B,rr}^s}{4\rho_{B,rr}^s}, \quad (11)$$

where the superscript s denotes a steady-state solution. $\Delta_{A(B),\text{eff}}^s$ is defined as in (8) and (9) by replacing $\rho_{A(B),rr}$ with $\rho_{A(B),rr}^s$. We find that Eqs. (10) and (11) can give nine pairs of roots ($\rho_{A,rr}^s$ and $\rho_{B,rr}^s$), in which only the real ones with values belonging to $[0,0.5]$ are physical, since for a single two-level atom the excitation probability saturates at 0.5 [37]. The stability of these roots can be tested by adding small perturbations and seeing whether the system can eventually be settled with these solutions. A detailed description of studying the stability criterion is presented elsewhere, e.g., the Supplementary Material to Ref. [15].

We classify all the dynamical phases according to the number of steady-state solutions as well as their dynamical features. As summarized in Table I, the total numbers of physical roots (PRN) are displayed in the first row of data, and the numbers of stable (SRN) and unstable (USRN) roots, in the second and third rows of data, respectively. If $\text{SRN} > \text{USRN}$, the dynamical phase is a stable phase; if $\text{SRN} < \text{USRN}$, it is an unstable phase. With the given parameters, in the current scheme we find a total of three stable and five unstable phases. Stable phases include the antiferromagnetic phase (labeled 1AF), with $\text{SRN} = 1$ and $\text{USRN} = 0$; the bistable antiferromagnetic phase (labeled 2AF), with $\text{SRN} = 2$ and $\text{USRN} = 1$; and the tristable antiferromagnetic phase (labeled 3AF), with $\text{SRN} = 3$ and $\text{USRN} = 2$. The five unstable phases are, respectively, labeled CH1, CH2, CH3, CH4, and CH5, and their SRN and USRN are listed in Table I. In the following discussion, we show that the dynamics of these stable phases always settles on one of the stable roots in all cases. However, the dynamics of the unstable phases is quite different. In the weak-interaction case, where the RRIs are

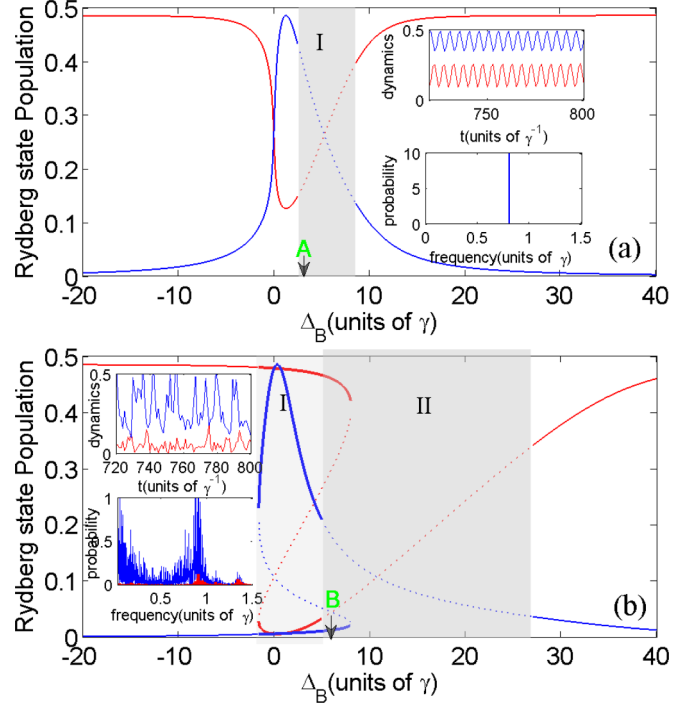


FIG. 2. (Color online) Stationary solutions $\rho_{A,rr}^s$ (red curves) and $\rho_{B,rr}^s$ (blue curves) as a function of detuning Δ_B when atoms A are assumed to be resonantly excited. (a) Weak-interaction case with $U_{AB} = 10$ and $\Omega = 2$; (b) strong-interaction case with $U_{AB} = 50$ and $\Omega = 2$. Stable and unstable solutions, respectively, are shown by solid and dotted curves. Insets in (a): The regular oscillatory dynamics and its single-frequency spectrum are observed at $\Delta_B = 3.0$, labeled “A” in the figure. Insets in (b): The chaotic dynamics and its continuous frequency spectrum are observed at $\Delta_B = 6.0$, labeled “B” in the figure. The initial condition is $\rho_{A,rr}^{t=0} = \rho_{B,rr}^{t=0} = 0.1$. The decay rate γ is the frequency unit.

comparable to or lower than the optical coupling strength, the unstable phases tend to show simply oscillatory dynamics, while in the strong-interaction case, in which the RRIs play the dominant roles, that is, $U_{AB} \gg \Omega_A, \Omega_B$, the system dynamics easily tends to be chaotic. The significant difference between the chaotic dynamics and the ordinary oscillatory dynamics is the continuous frequency spectrum without any characteristic frequency as shown in the insets in Fig. 2. Besides, we note that although it is demanding to implement, for phases CH3, CH4, and CH5, if the system is initially prepared properly, very close to their stable roots, the dynamics may also be stable and without oscillation.

In what follows we discuss the conditions of the emergence of these phases and study their changes with and without the effect of NNN RRIs by numerically simulating the system dynamics. Before this, we have to make a realistic estimation of all parameters required in the calculation. We use the decay rate γ as the frequency unit and assume the condition $\Omega_A = \Omega_B = \Omega$ with $\Omega = 10.0$ for strong-optical-coupling cases and $\Omega = 2.0$ for weak-coupling cases. In addition, strong and weak NN RRIs are represented by $U_{AB} = 50.0$ and $U_{AB} = 10.0$, respectively. The validity of these parameters can be verified by assuming that $\gamma = 0.1$ MHz; the resulting RRIs are $U_{AB} = 5.0$ or 1.0 MHz using the lattice spacing

$d = 3.84$ or $5.0 \mu\text{m}$. The required vdW interaction coefficient is $C_6^{(ij)} = 16 \text{ GHz } \mu\text{m}^6$, as suggested in Ref. [38].

III. PHASE DIAGRAM WITHOUT NNN RRIs

In this section we focus on the case without the impact of NNN RRIs, i.e., $U_{AA} = U_{BB} = 0$. In experiments, NN RRIs can be controlled directly by changing the interatomic distance [29] and the detunings Δ_A and Δ_B can be easily adjusted by changing the laser frequencies. We first fix $\Delta_A = 0$ (atom A is resonantly excited) and tune Δ_B from -20 to 40 to see the change in the steady Rydberg population of different atom species given by Eqs. (10) and (11).

In Fig. 2 we present the stationary Rydberg state populations with respect to Δ_B , with the weak-interaction case ($U_{AB} = 10.0$ and $\Omega = 2$) in Fig. 2(a) and the strong-interaction case ($U_{AB} = 50.0$ and $\Omega = 2$) in Fig. 2(b). Stable and unstable dynamical phases are, respectively, represented by solid and dotted curves. For the weak-interaction case when $\Delta_B < 0$ or $\Delta_B > 8.5$, corresponding to the far-off-resonance cases evaluated by the effective detuning $\Delta_{B,\text{eff}}^s$, there exists merely the 1AF phase with its dominant Rydberg probability in atom A. As Δ_B grows from negative to small positive values, we find that the increase in $\rho_{B,rr}^s$ will make $\Delta_{A,\text{eff}}^s (\propto -U_{AB}\rho_{B,rr}^s)$ nonzero, which further yields the excitation probability exchange between atom A and atom B. However, as Δ_B increases to regime I, where $\Delta_{A,\text{eff}}^s$ and $\Delta_{B,\text{eff}}^s$ are comparable, the steady-state solutions are found to become unstable, labeled by the oscillatory phase CH1. In this case the system dynamics can be characterized by the single-frequency oscillations due to the presence of weak Rydberg interactions, as displayed in the inset in Fig. 2(a). This finding shows similar results to the single-species atom case, in which the dynamics of the system will be periodically oscillating if its corresponding steady-state solutions become unstable [see Fig. 2(b) in Ref. [15]].

We now investigate the strong-interaction case, in which the Rydberg blockade effect could play a significant role in the system dynamics. Similarly to the result in the weak-interaction case, at a negative or large positive Δ_B the system tends to stay in the 1AF phase. We then pay more attention to the center region, where $\Delta_{A,\text{eff}}^s \approx \Delta_{B,\text{eff}}^s$ is satisfied. This region can be divided into two parts.

In part I there exists only the 2AF phase, with two stable roots ($\rho_{A,rr}^s > \rho_{B,rr}^s$ and $\rho_{A,rr}^s < \rho_{B,rr}^s$) as well as one unstable root. The system will selectively settle on one of the two stable roots, accounting for the initial population preparations.

In part II the phase transitions from CH3 to CH1. CH3, corresponding to one stable and two unstable roots, is an unstable phase. Except that initially the system is prepared in a state near the stable root, the system dynamics is oscillatory and trends to be chaotic in the strong-interaction limit $U_{AB} \gg \Omega$, characterized by a continuous spectrum in the frequency domain as presented in the insets in Fig. 2(b). As Δ_B increases, no stable solution is supported by the given parameters and the phase changes to CH1. However, owing to the strong RRIs, this CH1 phase also shows chaotic dynamics instead of the regular oscillations in the weak-interaction cases.

In Fig. 3 we plot the phase diagrams in a two-dimensional (2D) parameter space of Δ_A and Δ_B , performing a comparison

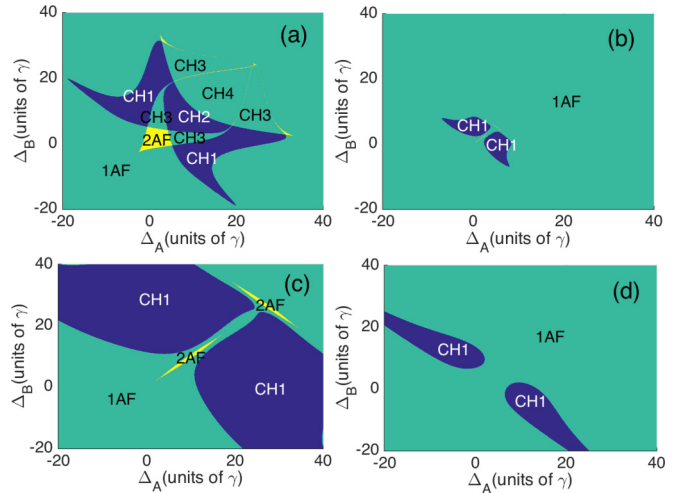


FIG. 3. (Color online) Phase diagram in the 2D parameter space (Δ_A, Δ_B). Left-column diagrams are obtained from the strong-interaction case with (a) $U_{AB} = 50.0$, $\Omega = 2.0$ and (c) $U_{AB} = 50.0$, $\Omega = 10.0$. Right-column diagrams are from the weak-interaction case with (b) $U_{AB} = 10.0$, $\Omega = 2.0$ and (d) $U_{AB} = 10.0$, $\Omega = 10.0$. γ is the frequency unit.

among the four cases. In the case in Fig. 3(b), where the NN interaction strength $U_{AB} = 10$ and the optical coupling $\Omega = 2$, we find that the phase diagram is mainly occupied by the stable phase 1AF, and the unstable phase CH1 survives only in two narrow areas where Δ_A and Δ_B have opposite signs. When the optical coupling increases enough to be comparable to the interaction strength, as in Fig. 3(d), with $U_{AB} = \Omega = 10$, the regions of CH1 expand, but 1AF is still the dominant phase. We stress that due to the low ratio of interaction U_{AB} and Ω , in both cases, Figs. 3(b) and 3(d), the dynamics of the unstable phase CH1 is only normal oscillation rather than chaos. When we turn to a case with a very strong interaction strength and a weak optical coupling, such as that in Fig. 3(a), with $U_{AB} = 50$ and $\Omega = 2$, besides phases 1AF and CH1, the phase diagram shows a large number of unique phases, including the bistable phase 2AF and unstable phases CH2, CH3, and CH4. Moreover, we find that the dynamics of these unstable phases is no longer regular oscillations, but chaotic oscillations without any characteristic frequencies, which is similar to the case shown in the inset in Fig. 2(b). In the case in Fig. 3(c) we keep $U_{AB} = 50$ and increase Ω to 10. Due to the narrowed gap between the interaction strength and the optical coupling, the phase diagram degenerates and resembles those for the cases in Figs. 3(b) and 3(d). CH1 becomes the only survival unstable phase and 2AF shrinks into narrow areas where the detunings of atoms A and B are almost equal. Also, the dynamics of CH1 returns to normal oscillation, which reconfirms that the condition for arising chaos in unstable phases is the strong-interaction limit $U_{AB} \gg \Omega$.

IV. PHASE DIAGRAM WITH CONSIDERABLE NNN RRIs

In the following, we consider the effect of NNN RRIs on the phase diagram of the system. For simplicity, we assume that the long-range NNN RRIs for atoms of different species

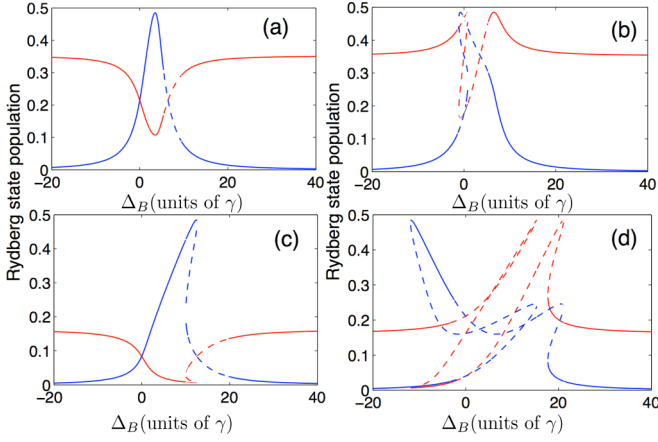


FIG. 4. (Color online) Stationary Rydberg population $\rho_{A,rr}^s$ (red curves) and $\rho_{B,rr}^s$ (blue curves) with respect to Δ_B . Stable and unstable solutions are represented by solid and dashed curves, respectively. The long-range NNN interaction is (a, c) $U_0 = 0.5U_{AB}$ and (b, d) $U_0 = -0.5U_{AB}$. (a, b) Weak-interaction case with $U_{AB} = 10.0$ and $\Omega = 2.0$; (c, d) strong-interaction case with $U_{AB} = 50.0$ and $\Omega = 2.0$. Δ_A is fixed at 0 in all cases.

are equal and are half the NN RRI, that is, $U_{AA} = U_{BB} = U_0 = \pm 0.5U_{AB}$. Plus and minus signs represent repulsive and attractive NNN RRI, respectively.

Figure 4 shows the change in the steady-state Rydberg populations $\rho_{A,rr}^s$ and $\rho_{B,rr}^s$ when the RRI between NNN-site atoms are included. Figures 4(a) and 4(c) show the weak-NN-interaction case ($U_{AB} = 10$) and the strong-interaction case ($U_{AB} = 50$), respectively. In both cases we set the NNN interaction to be repulsive ($U_0 = 0.5U_{AB}$) and the detuning $\Delta_A = 0$. The arrangement is similar for Figs. 4(b) and 4(d), but with an attractive NNN interaction. Compared with Fig. 2, which neglects the effect of NNN interactions, we observe a significant decrease in population in atom A (shown by red curves), particularly in the region of large detuning $|\Delta_B|$, because according to Eq. (8), a repulsive U_0 could make the effective detuning $\Delta_{A,\text{eff}}^s$ more negative in addition to the existing negative shift caused by the NN interaction term. In the middle region where Δ_B is positive but small, we numerically find $\Delta_{A,\text{eff}}^s \approx \Delta_{B,\text{eff}}^s$, and a repulsive NNN interaction can partially compensate for the detunings (e.g., Δ_B can be compensated by $U_0\rho_{B,rr}^s$ if $\rho_{A,rr}^s$ is small), which gives rise to a reduction in the number of unstable or multistable (bistable or tristable) stationary solutions.

However, turning to the attractive case ($U_0 < 0$) we find that it changes significantly. Due to the different signs of the NNN interaction and the NN interaction, the effective steady-state atomic detunings can be rewritten as

$$\Delta_{A,\text{eff}}^s = \Delta_A + (|U_0|\rho_{A,rr}^s - U_{AB}\rho_{B,rr}^s), \quad (12)$$

$$\Delta_{B,\text{eff}}^s = \Delta_B + (|U_0|\rho_{B,rr}^s - U_{AB}\rho_{A,rr}^s). \quad (13)$$

Differently from the repulsive case, here the frequency shifts caused by the NNN interaction and the NN interaction are opposite. As demonstrated in Fig. 4(b), where $U_{AB} = 10.0$ is relatively weak, we see that $\rho_{A,rr}^s$ can touch the peak value 0.5 again when the frequency shifts in the effective detuning $\Delta_{A,\text{eff}}^s$

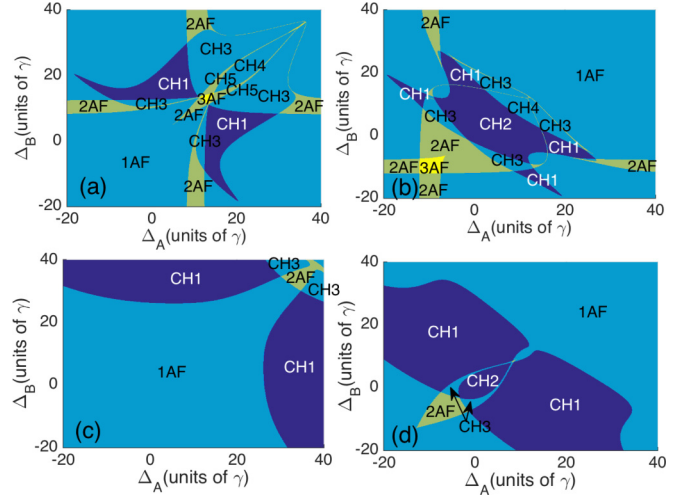


FIG. 5. (Color online) Phase diagram in (Δ_A, Δ_B) space by the effect of repulsive and attractive NNN RRI. (a, b) Plots correspond to the case in Fig. 3(a), where $U_{AB} = 50.0$ and $\Omega = 2.0$; (c, d) to the case in Fig. 3(c), where $U_{AB} = 50.0$ and $\Omega = 10.0$. Correspondingly, we use the NNN RRI $U_0 = 0.5U_{AB}$ (repulsive) in (a) and (c) and $U_0 = -0.5U_{AB}$ (attractive) in (b) and (d).

caused by the NN interaction and NNN interaction cancel each other. As $|\Delta_B|$ approaches 0, $\rho_{A,rr}^s$ becomes unstable and shows a sharp drop, in which a clear population exchange occurs between atom A and atom B. This is because atom B is almost resonantly excited instead of atom A when $\Delta_{B,\text{eff}}^s$ is close to 0, due to the offset effect of the NN and the NNN interactions in $\Delta_{B,\text{eff}}^s$. With a larger U_{AB} value this will, further, lead to multiple unstable solutions, as displayed in Fig. 4(d), where the dynamics of the system becomes more complex and elusive.

Mapping these results into the 2D parameter space of Δ_A and Δ_B and comparing them with the cases in Figs. 3(a) and 3(c), we more clearly find the change in dynamical phases under the impact of the considerable NNN RRI. As shown in Fig. 5, generally speaking, dependent on the NNN RRI being repulsive ($U_0 > 0$) or attractive ($U_0 < 0$), all the unique phases except the 1AF phase will diffuse from or converge to the center region where $\Delta_A \approx \Delta_B \approx 0$. As stated in the previous paragraph, this is due to the additive effect of the repulsive NNN interaction and the NN interaction on the effective detunings $\Delta_{A,\text{eff}}^s$ and $\Delta_{B,\text{eff}}^s$. A typical example is shown in Fig. 5(a), whose parameters are the same as in Fig. 3(a), except that the NNN interaction $U_0 = 0.5U_{AB}$. We find that the bistable phase 2AF occurs mainly when Δ_A or Δ_B is far off-resonance, in order to compensate for the large difference between $\rho_{A,rr}^s$ and $\rho_{B,rr}^s$. A new tristable phase, 3AF, arises due to the multiple steady-state solutions caused by the inclusion of NNN RRI. Other unstable phases are all dispersedly distributed in the parameter space and the CH2 phase disappears. In Figs. 5(c) and 5(d), where both the NN interaction and the optical coupling are large, the number of phases dramatically decreases, but compared with Fig. 3(c) we still find similar diffusion and convergence effects caused by the NNN interactions.

Finally, we stress again the properties of all unique phases possibly obtained in our scheme when both NN and NNN RRI are considered. A related result is also reported in Table I. The

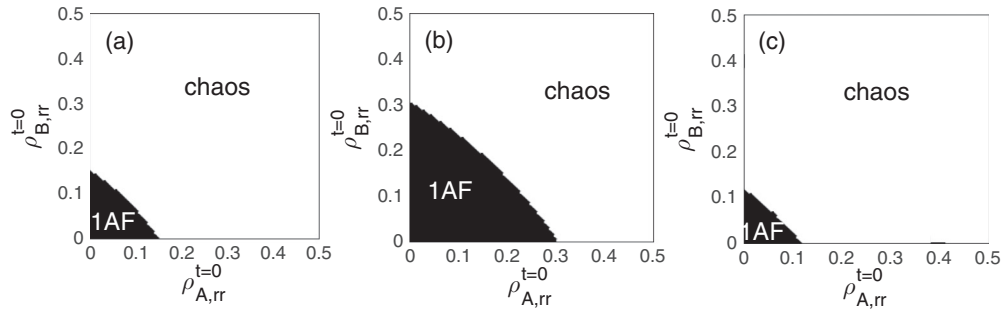


FIG. 6. Final-state distribution in the unstable-phase CH4 as functions of $\rho_{A,rr}^{t=0}$ and $\rho_{B,rr}^{t=0}$. Cases (a) without NNN interactions [according to Fig. 3(a); $U_0 = 0$], (b) with repulsive NNN interactions [according to Fig. 5(a); $U_0 = 0.5U_{AB}$], and (c) attractive NNN interactions [according to Fig. 5(b); $U_0 = -0.5U_{AB}$]. Detunings are chosen to be $\Delta_A = \Delta_B = 15.0$ (a), 23.0 (b), and 10.0 (c).

three stable phases are (i) 1AF, which includes one stable solution and no unstable solution, so that the system finally stays in the stable solution; (ii) 2AF, which includes two stable solutions and one unstable solution, so that the system tends to stop on the one near its initial state; and (iii) 3AF, which includes three stable solutions and two unstable solutions, so that the system will also choose the nearest one to settle. In addition, the five unstable phases are labeled CH n ($n = 1, 2, 3, 4, 5$), where USRN is larger than SRN. Except when initially the system is very close to the stable roots of CH n ($n = 3, 4, 5$), the system will keep evolving and not settle on any stationary state. In the strong-interaction case, where the RRI plays a dominant role, the system may show complex chaotic dynamics that is very sensitive to the initial prepared population in the Rydberg state; in the weak-interaction case, with the RRI comparable to the optical coupling strength, these unstable phases will lead to regular oscillatory dynamics for the system.

V. INFLUENCE OF NNN RRIs ON THE CHAOTIC PHASE

In the strong-interaction case with $U_{AB} \gg \Omega$ we have found that the dynamics of the system can show chaotic properties if the dynamical phase becomes unstable. Due to the high sensitivity of the chaos, it becomes a good candidate to show the dramatic influence of NNN RRIs on our model. Here, we use CH4 (SRN = 1, USRN = 4) as an example to see the final state. By directly solving the dynamical evolution of motional equations (4)–(7) we can determine which phase the system will finally evolve into. In the calculation, we assume that the initial preparations $\rho_{A,rr}^{t=0}$ and $\rho_{B,rr}^{t=0}$ are fully adjustable.

Figures 6(a)–6(c) display the final state of the system when the initial preparations in the Rydberg states are varied. Since CH4 contains one stable solution the system may also possibly stay on it when the initial prepared population is close to that stable solution. Thus, when the system settles on CH4 its real dynamics shows two different cases. One is a stable steady state like 1AF (“1AF”) and the other is unstable chaos (“chaos”). Figures 6(a)–6(c) respectively consider the cases without and with repulsive and attractive Rydberg interactions between two NNN-site atoms. We find, comparing to Fig. 6(a), that a repulsive NNN interaction [see Fig. 6(b)] will make the system more stable against chaos. It is more likely to show a stable dynamics under the environment of the chaotic phase CH4.

However, when the NNN interaction is attractive, as plotted in Fig. 6(c), we find that the area in the parameter space that presents stable dynamics clearly shrinks dramatically. Except when $\rho_{A,rr}^{t=0}$ and $\rho_{B,rr}^{t=0}$ are both close to the exact steady-state solutions [$\rho_{A,rr}^s = \rho_{B,rr}^s = 0.046$], the dynamics of the system will be totally chaotic and unmeasurable. This finding is implied in Fig. 4(d), in which multiple unstable roots are represented because $U_0 < 0$.

VI. CONCLUSIONS

We represent a rich variety of dynamical phases of a chain of two-species Rydberg atoms held in a 1D optical lattice, where the optical transition between the atomic ground state and the high-lying Rydberg state is performed by one-photon excitation. In particular, except for the NN Rydberg interaction between atoms of different species, the long-range NNN interactions between atoms of the same species are also considered. We show that the phase diagrams change a lot when the long-range interaction is included. Especially, repulsive or attractive long-range interactions can give rise to a clear diffusing or converging effect on the original phase diagrams without them. For instance, a repulsive NNN RRI can help to stabilize the system against chaotic dynamics. In addition, we also study the real final state of the chaotic phase in the strong-interaction limit and illustrate its sensitivity to the initial atomic preparations in the Rydberg state. Most of these results and phenomena are novel, but we stress that when $\Delta_A = \Delta_B$ and the NNN RRI vanishes, our results will tend to be consistent with the previous findings from a Rydberg system of single-species atoms [15].

ACKNOWLEDGMENTS

This work was supported by the National Basic Research Program of China (973 Program) under Grant No. 2011CB921604, the NSFC under Grants No. 11474094, No. 11104076 and No. 11234003, and the Specialized Research Fund for the Doctoral Program of Higher Education Grant No. 20110076120004.

- [1] D. Jaksch, C. Bruder, J. I. Cirac, C. W. Gardiner, and P. Zoller, Cold Bosonic Atoms in Optical Lattices, *Phys. Rev. Lett.* **81**, 3108 (1998).
- [2] I. Bloch, Ultracold quantum gases in optical lattices, *Nat. Phys.* **1**, 23 (2005).
- [3] O. Morsch and M. Oberthaler, Dynamics of Bose-Einstein condensates in optical lattices, *Rev. Mod. Phys.* **78**, 179 (2006).
- [4] M. Lewenstein, A. Sanpera, V. Ahufinger, B. Damski, A. Sen De, and U. Sen, Ultracold atomic gases in optical lattices: Mimicking condensed matter physics and beyond, *Adv. Phys.* **56**, 243 (2007).
- [5] M. Lewenstein, A. Sanpera, and V. Ahufinger, *Ultracold Atoms in Optical Lattices: Simulating Quantum Many-Body Systems* (Oxford University Press, New York, 2012).
- [6] I. Bloch, J. Dalibard, and W. Zwerger, Many-body physics with ultracold gases, *Rev. Mod. Phys.* **80**, 885 (2008), and references therein.
- [7] S. E. Anderson, K. C. Younge, and G. Raithel, Trapping Rydberg Atoms in an Optical Lattice, *Phys. Rev. Lett.* **107**, 263001 (2011).
- [8] T. F. Gallagher and P. Pillet, Dipole-dipole interactions of Rydberg atoms, *Adv. At. Mol. Opt. Phys.* **56**, 161 (2008).
- [9] D. Comparat and P. Pillet, Dipole blockade in a cold Rydberg atomic sample, *J. Opt. Soc. Am. B* **27**, A208 (2010).
- [10] T. Pohl, E. Demler, and M. D. Lukin, Dynamical Crystallization in the Dipole Blockade of Ultracold Atoms, *Phys. Rev. Lett.* **104**, 043002 (2010).
- [11] H. Weimer, M. Müller, I. Lesanovsky, P. Zoller, and H. P. Büchler, A Rydberg quantum simulator, *Nat. Phys.* **6**, 382 (2010).
- [12] M. Viteau, M. G. Bason, J. Radogostowicz, N. Malossi, D. Ciampini, O. Morsch, and E. Arimondo, Rydberg Excitations in Bose-Einstein Condensates in Quasi-One-Dimensional Potentials and Optical Lattices, *Phys. Rev. Lett.* **107**, 060402 (2011).
- [13] P. Schaub, M. Cheneau, M. Endres, T. Fukuhara, S. Hild, A. Omran, T. Pohl, C. Gross, S. Kuhr, and I. Bloch, Observation of spatially ordered structures in a two-dimensional Rydberg gas, *Nature* **491**, 87 (2012).
- [14] C. Carr, R. Ritter, C. G. Wade, C. S. Adams, and K. J. Weatherill, Nonequilibrium Phase Transition in a Dilute Rydberg Ensemble, *Phys. Rev. Lett.* **111**, 113901 (2013).
- [15] T. E. Lee, H. Häffner, and M. C. Cross, Antiferromagnetic phase transition in a nonequilibrium lattice of Rydberg atoms, *Phys. Rev. A* **84**, 031402 (2011); I. Lesanovsky, Excited atoms spin out of equilibrium, *Physics* **4**, 71 (2011).
- [16] J. Qian, G. Dong, L. Zhou, and W. Zhang, Phase diagram of Rydberg atoms in a nonequilibrium optical lattice, *Phys. Rev. A* **85**, 065401 (2012).
- [17] J. Qian, L. Zhou, and W. Zhang, Quantum phases of strongly interacting Rydberg atoms in triangular lattices, *Phys. Rev. A* **87**, 063421 (2013).
- [18] M. Hoening, W. Abdussalam, M. Fleischhauer, and T. Pohl, Antiferromagnetic long-range order in dissipative Rydberg lattices, *Phys. Rev. A* **90**, 021603 (2014).
- [19] B. Olmos, D. Yu, and I. Lesanovsky, Steady-state properties of a driven atomic ensemble with nonlocal dissipation, *Phys. Rev. A* **89**, 023616 (2014).
- [20] C.-K. Chan, T. E. Lee, and S. Gopalakrishnan, Limit-cycle phase in driven-dissipative spin systems, *Phys. Rev. A* **91**, 051601(R) (2015).
- [21] M. Höning, D. Muth, D. Petrosyan, and M. Fleischhauer, Steady-state crystallization of Rydberg excitations in an optically driven lattice gas, *Phys. Rev. A* **87**, 023401 (2013).
- [22] I. I. Beterov and M. Saffman, Rydberg blockade, Förster resonances, and quantum state measurements with different atomic species, *Phys. Rev. A* **92**, 042710 (2015).
- [23] C.-H. Hsueh, Y.-C. Tsai, K.-S. Wu, M.-S. Chang, and W.-C. Wu, Pseudospin orders in the supersolid phases in binary Rydberg-dressed Bose-Einstein condensates, *Phys. Rev. A* **88**, 043646 (2013).
- [24] R. C. Teixeira, C. Hermann-Avigliano, T. L. Nguyen, T. Cantat-Moltrecht, J. M. Raimond, S. Haroche, S. Gleyzes, and M. Brune, Microwaves Probe Dipole Blockade and van der Waals Forces in a Cold Rydberg Gas, *Phys. Rev. Lett.* **115**, 013001 (2015).
- [25] D. Barredo, H. Labuhn, S. Ravets, T. Lahaye, A. Browaeys, and C. S. Adams, Coherent Excitation Transfer in a Spin Chain of Three Rydberg Atoms, *Phys. Rev. Lett.* **114**, 113002 (2015).
- [26] R. Scelle, T. Rentrop, A. Trautmann, T. Schuster, and M. K. Oberthaler, Motional Coherence of Fermions Immersed in a Bose Gas, *Phys. Rev. Lett.* **111**, 070401 (2013).
- [27] T. Ramos, H. Pichler, A. J. Daley, and P. Zoller, Quantum Spin Dimers from Chiral Dissipation in Cold-Atom Chains, *Phys. Rev. Lett.* **113**, 237203 (2014).
- [28] K. Singer, J. Stanojevic, M. Weidemüller, and R. Côté, Long-range interactions between alkali Rydberg atom pairs correlated to the ns-ns, np-np and nd-nd asymptotes, *J. Phys. B* **38**, S295 (2005).
- [29] L. Béguin, A. Vernier, R. Chicireanu, T. Lahaye, and A. Browaeys, Direct Measurement of the van der Waals Interaction between Two Rydberg Atoms, *Phys. Rev. Lett.* **110**, 263201 (2013).
- [30] B. Olmos, W. Li, S. Hofferberth, and I. Lesanovsky, Amplifying single impurities immersed in a gas of ultracold atoms, *Phys. Rev. A* **84**, 041607 (2011).
- [31] H. Zoubi, Van der Waals interactions among alkali Rydberg atoms with excitonic states, *J. Phys. B: At. Mol. Opt. Phys.* **48**, 185002 (2015).
- [32] S. Diehl, A. Micheli, A. Kantian B. Kraus, H. P. Büchler, and P. Zoller, Quantum states and phases in driven open quantum systems with cold atoms, *Nat. Phys.* **4**, 878 (2008).
- [33] S. Diehl, A. Tomadin, A. Micheli, R. Fazio, and P. Zoller, Dynamical Phase Transitions and Instabilities in Open Atomic Many-Body Systems, *Phys. Rev. Lett.* **105**, 015702 (2010).
- [34] A. Tomadin, S. Diehl, and P. Zoller, Nonequilibrium phase diagram of a driven and dissipative many-body system, *Phys. Rev. A* **83**, 013611 (2011).
- [35] C. Ates, T. Pohl, T. Pattard, and J. M. Rost, Antiblockade in Rydberg Excitation of an Ultracold Lattice Gas, *Phys. Rev. Lett.* **98**, 023002 (2007).
- [36] T. Amthor, C. Giese, C. S. Hofmann, and M. Weidemüller, Evidence of Antiblockade in an Ultracold Rydberg Gas, *Phys. Rev. Lett.* **104**, 013001 (2010).
- [37] D. Petrosyan, M. Höning, and M. Fleischhauer, Spatial correlations of Rydberg excitations in optically driven atomic ensembles, *Phys. Rev. A* **87**, 053414 (2013).
- [38] D. W. Schönleber, M. Gärttner, and J. Evers, Coherent versus incoherent excitation dynamics in dissipative many-body Rydberg systems, *Phys. Rev. A* **89**, 033421 (2014).